Polarization-singular structure in laser images of phase-inhomogeneous layers to diagnose and classify their optical properties

Yu.O. Ushenko, I.Z. Misevich, A.P. Angelsky, V.T. Bachinsky, O.Yu. Telen'ga, O.I. Olar
Yuri Fedkovych Chernivtsi National University,
2 Kotsybynsky str., 58012 Chernivtsi, Ukraine

Abstract. Adduced in this work are the results of investigation aimed at analysis of coordinate distributions for azimuths and ellipticity of polarization (polarization maps) in laser images of three types of phase-inhomogeneous layers (PhIL), namely: rough, ground and bulk scattering layers. To characterize polarization maps for all the types of PhIL, the authors have offered to use three groups of parameters: statistical moments of the first to fourth orders, autocorrelation functions, logarithmic dependences for power spectra related to distributions of azimuths and ellipticity of polarization inherent to PhIL laser images. Ascertained are the criteria for diagnostics and classification of PhIL optical properties.

Keywords: polarization, rough surface, phase-inhomogeneous layer, statistical moment, autocorrelation.

1. Introduction

By tradition, the processes of transforming optical radiation of phase-inhomogeneous objects and media are considered, as a rule, in a statistical approach (theory of radiation transfer [1], Monte-Carlo modeling [2]). Among the most spread traditional methods for studying the scattered light fields, one can separate the following independent directions: "scalar" (photometry and spectrophotometry) [3, 4] and "vector" (polarization nephelometry, Mueller-matrix optics) [5 - 13]. Using these approaches, determined are interrelations between the sets of statistical moments of the 1-st to 4-th orders, correlation functions, fractal dimensionalities that characterize phase-inhomogeneous or rough surfaces and coordinate distributions for phases, azimuths and ellipticity of polarization in their laser images [14 - 22].

In parallel with traditional statistical investigations, formed in recent 10 to 15 years is the new optical approach to describe a structure of polarizationally inhomogeneous fields in the case of scattered coherent radiation. The main feature of this approach is the analysis of definite polarization states to determine the whole structure of coordinate distributions for azimuths and ellipticities of polarization. The so-called polarization singularities are commonly used as these states [23 – 43]:

- states with linear polarization when the direction of rotation for the electric field vector is indefinite, the so-called L-points;
- circularly-polarized states when the azimuth of polarization for the electric field vector is indefinite, the so-called C-points.

This work is aimed at ascertaining the possibilities to diagnose and classify phase-inhomogeneous layers (PhIL) of various types (surface-scattering, subsurface-scattering and bulk-scattering ones) by determination values and ranges for changing the statistical (moments of the 1-st to 4-th orders), correlation (autocorrelation functions) and fractal (logarithmic dependences for power spectra) parameters that characterize coordinate distributions for polarization-singular states in PhIL laser images.

2. Main model conceptions and analytical relations

As a base for analytical description of processes providing formation of polarization-inhomogeneous images for various types of PhIL, we have used the

model conceptions developed in the works [5, 14, 19, 21, 22]:

- surface-scattering PhIL is a rough surface consisting of an ensemble of quasi-plane, chaotically oriented micro-areas with optical dimensions $l \succ \lambda$;
- PhIL with surface and subsurface scattering – ground glass with rough external and subsurface (cracked layer) components;
- PhIL with bulk scattering – milky glass MC20 of a various optical thickness.

2.1. Mechanisms providing formation of polarization-inhomogeneous images for rough surface

As an example of PhIL with surface scattering, we have considered replicas (exact prints of the surface of ground glass) made of optically isotropic composite material. The range of changes in geometric sizes (l) of micro-roughness (micro-areas) for these rough surfaces corresponds to 2 to 60 µm. Optical properties of each micro-area are exhaustively characterized with the Jones operator of the following look

$$\{R\} = \begin{Vmatrix} 1 & 0 \\ 0 & p_y/p_x \end{Vmatrix}. \tag{1}$$

It is possible to show that within the sizes ($\Delta x, \Delta y$) of one micro-area there takes place the change of polarization azimuth α inherent to the refracted plane-polarized laser wave with the initial azimuth α_0

$$\alpha(\Delta x, \Delta y) = arctg \frac{p_y U_{0y}}{p_x U_{0x}} = arctg[\Delta p_{xy} tg\alpha_0], \tag{2}$$

where U_{0x}, U_{0y} are orthogonal components of the amplitude U_0; p_x, p_y - Fresnel amplitude coefficients for transmission [5].

Thus, in the approach of one-fold scattering the polarization image of rough surface may be considered as coordinate-distributed parts of L-polarized states.

2.2. Model structure of PhIL with surface and subsurface components – ground surfaces

As examples of these PhIL, we have considered plane-parallel layers of glass K8 ($n = 1.47$) ground with abrasive powders of various grades (M5, M10, M28 and M40 with statistically averaged sizes 5 to 8, 10 to 15, 25 to 30 and 40 to 50 µm, respectively).

The process providing formation of a local polarization state can be considered as superposition of "influences" of an optically strained subsurface cracked layer as well as the surface rough micro-relief one disposed in sequence. From the analytical viewpoint, this scenario can be described by superposition $\{F\}$ of the Jones matrix operators for these partial layers (cracked $\{T\}$ and surface $\{R\}$)

$$\{F\} = \{R\}\{T\} = \begin{Vmatrix} f_{11} & f_{12} \\ f_{21} & f_{22} \end{Vmatrix} =$$
$$= \begin{Vmatrix} (r_{11}t_{11} + r_{12}t_{21}); & (r_{11}t_{12} + r_{12}t_{22}); \\ (r_{21}t_{11} + r_{22}t_{21}); & (r_{21}t_{12} + r_{22}t_{22}) \end{Vmatrix}, \tag{3}$$

$$\{T\} = \begin{Vmatrix} t_{11} & t_{12} \\ t_{21} & t_{22} \end{Vmatrix} =$$
$$= \begin{Vmatrix} [\cos^2\gamma + \sin^2\gamma \exp(i\delta)]; & [\cos\gamma\sin\gamma \exp(i\delta)]; \\ [\cos\gamma\sin\gamma \exp(i\delta)]; & [\sin^2\gamma + \cos^2\gamma \exp(i\delta)] \end{Vmatrix}. \tag{4}$$

Here, γ is the direction of the optical axis inherent to strained (crystalline) bulk; δ - phase shift between orthogonal components ($U_x; U_y$) of the amplitude (U) of laser wave with the wavelength λ that arises as a consequence of birefringence in the matter Δn.

If taking into account the relations (1), (3) and (4), it follows that within the limits ($\Delta x, \Delta y$) of a local bulk created by the micro-area and micro-crack of rough surface, formed is an elliptically polarized part of the object field (Fig. 2b) with the following parameters

$$\tilde{\alpha}(\Delta x, \Delta y) = ar\cos\left(\sin\delta \middle/ \cos 2\left(arctg\left\{\left[\frac{(f_{21} + f_{22})^2}{(f_{11} + f_{12})^2}\right]tg\alpha_0\right\}\right)\right); \tag{5}$$

$$\tilde{\beta}(\Delta x, \Delta y) = \arcsin\left(tg\delta \middle/ \sin 2\left(arctg\left\{\left[\frac{(f_{21} + f_{22})^2}{(f_{11} + f_{12})^2}\right]tg\alpha_0\right\}\right)\right). \tag{6}$$

As it follows from the analytical relations (5) and (6), interaction of the plane-polarized (α_0) wave with the PhIL of this type provides formation of a polarization-inhomogeneous laser image. Among the whole set of values $(\tilde{\alpha}; \tilde{\beta})$, formation of L and $\pm C$ polarization states seems to be very probable

$$L- \Leftrightarrow \delta(\Delta x, \Delta y) = q\pi, \quad q = 1; 2, \dots; \qquad (7)$$

$$\pm C- \Leftrightarrow tg\,\delta(\Delta x, \Delta y) =$$

$$= \sin 2\left(arctg\left\{ \left[\frac{(f_{21}(\Delta x, \Delta y) + f_{22}(\Delta x, \Delta y))^2}{(f_{11}(\Delta x, \Delta y) + f_{12}(\Delta x, \Delta y))^2} \right] tg\,\alpha_0 \right\} \right). \quad (8)$$

2.3. Polarization structure of laser fields inherent to PhIL with bulk scattering

When analyzing the processes of interaction of laser radiation with these PhIL, we have used the method of superposition of the Jones matrix operators (3) for the set of sequentially disposed optically-thin layers

$$\{\Phi\} = \{\Phi^{(p)}\}\{\Phi^{(p-1)}\} \times \dots \times \{\Phi^{(1)}\} \qquad (10)$$

Having calculated the set of Jones matrix elements ϕ_{qg} for an optically-thick PhIL, one can define analytical expressions (like to (5) – (6)) to find L and $\pm C$ polarization states in the laser image

$$L- \Leftrightarrow \delta^*(\Delta x, \Delta y) = q\pi, \quad q = 1; 2, \dots; \qquad (11)$$

$$\pm C- \Leftrightarrow tg\,\delta^*(\Delta x, \Delta y) =$$

$$= \sin 2\left(arctg\left\{ \left[\frac{(\phi_{21}(\Delta x, \Delta y) + \phi_{22}(\Delta x, \Delta y))^2}{(\phi_{11}(\Delta x, \Delta y) + \phi_{12}(\Delta x, \Delta y))^2} \right] tg\,\alpha_0 \right\} \right). \qquad (12)$$

Thus, the above analytical consideration (relations (1) to (12)) for various scenarios of transformation of laser radiation by PhIL in all the cases enabled to reveal the principled possibility of formation of polarization-singular states ($\beta = 0; \beta = \pm \frac{\pi}{4}$) in respective laser images.

In this work, to describe coordinate (x, y) distributions for polarization-singular ($L, \pm C$) states in laser images for all the types of PhIL

$$\begin{cases} V_4(x, y) = 0 \leftrightarrow L(\beta = 0); \\ V_4(x, y) = \pm 1 \leftrightarrow \pm C\left(\beta = \pm \frac{\pi}{4}\right) \end{cases} \qquad (13)$$

### 3. Experimental setup for polarimetric investigations

Our study of polarization-inhomogeneous laser images inherent to PhIL was performed using the optical scheme of a laser polarimeter (Fig. 1) [38 - 41]

Illumination was performed using a parallel beam ($\varnothing = 10^4$ μm) from a He-Ne laser ($\lambda = 0.6328$ μm) 1. The polarization illuminator (quarter-wave plates 3 and 5 as well as polarizer 4) were used to form various polarization states in the laser beam. Polarization images of PhIL 6 were projected using the micro-objective 7 into the plane of the light-sensitive area ($800\,pix \times 600\,pix$) in CCD camera 10. Turning the transmission axis of the analyzer 9 by the angles $\pm 45^0$ relatively to the direction of the highest velocity axis for the quarter-wave plate 8, wee could determine the intensities of right ($I_\otimes$) and left ($I_\oplus$) circularly polarized components for each separated pixel of CCD camera 10. It served as a base to calculate coordinate distributions of the fourth parameter in the Stokes vector $V_4(m \times n)$) describing the laser image of PhIL, if using the relation

$$V_4 \begin{pmatrix} r_{11}, \dots r_{1m} \\ \dots \dots \\ r_{n1}, \dots r_{nm} \end{pmatrix} = \frac{I_\otimes(r_{ik}) - I_\oplus(r_{ik})}{I_\otimes(r_{ik}) + I_\oplus(r_{ik})}. \qquad (14)$$

The two-dimensional array (14) was scanned along the horizontal direction $x \equiv 1, \dots, m$ with the step $\Delta x = 1\,pix$. Within the limits of each local sample $(1_{pix} \times n_{pix})^{(k=1,\ 2,\ \dots,\ m)}$, we calculated the amount (N) of characteristic values $V_4(k) = 0$, - ($N_L^{(k)}$) and $V_4(k) = \pm 1$, - ($N_{\pm C}^{(k)}$).

Thus, we determined the dependences $N_L(x) \equiv (N_L^{(1)}, N_L^{(2)}, \dots, N_L^{(m)})$ and $N_{\pm C}(x) \equiv (N_{\pm C}^{(1)}, N_{\pm C}^{(2)}, \dots, N_{\pm C}^{(m)})$ for amounts of polarization-singular $L-$ and $\pm C-$ points within the limits of a laser image for PhIL.
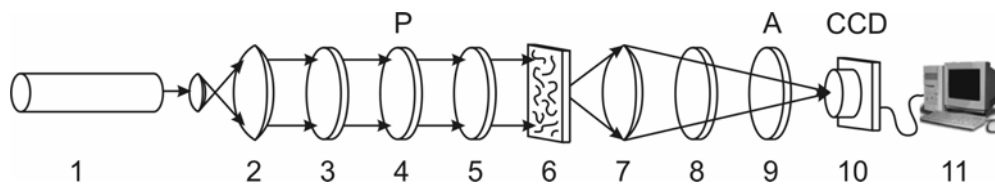
Fig. 1. Optical scheme of the polarimeter: 1 – He-Ne laser; 2 – collimator; 3, 5, 8 – quarter-wave plates; 4, 9 – polarizer and analyzer, respectively; 6 – object under investigation; 7 – micro-objective; 10 – CCD camera; 11 – personal computer.

4. Criteria to estimate polarization-inhomogeneous images of PhIL

Distributions $N_{L;\pm C}(x)$ for the amount of polarization-singular states in laser images of PhIL are characterized with the set of statistical moments of the 1-st to 4-th orders $Z_{j=1;2;3;4}$ calculated using the following relations [14]

$$Z_1 = \frac{1}{M}\sum_{i=1}^{M}\left|N_{L;\pm C}^{(i)}(x)\right|; Z_2 = \sqrt{\frac{1}{M}\sum_{i=1}^{M}\left[N_{L;\pm C}^{(i)}(x)\right]^2};$$

$$Z_3 = \frac{1}{Z_2^3}\frac{1}{M}\sum_{i=1}^{M}\left[N_{L;\pm C}^{(i)}(x)\right]^3; \quad Z_4 = \frac{1}{Z_2^2}\frac{1}{M}\sum_{i=1}^{M}\left[N_{L;\pm C}^{(i)}(x)\right]^4,$$
(15)

where $N = 800 \times 600$ is the amount of pixels in CCD camera 10 (Fig. 1).

Our analysis of the coordinate structure for $N_{L;\pm C}(x)$ distributions was based on the autocorrelation method by using the function [15, 19]

$$K_{L;\pm C}(\Delta x) = \lim_{m\to 0}\frac{1}{m}\int_1^m N_{L;\pm C}(x)N_{L;\pm C}(x-\Delta x)dx .$$
(16)

Here, $(\Delta x = 1 pix)$ is the step for changing the coordinate $x = 1 \div m$.

As correlation parameters that characterize the dependences $K_{L;\pm C}(\Delta x)$, we chose:

• correlation area $S_{L;\pm C}$

$$S_{L;\pm C} = \int_1^m K_{L;\pm C}(\Delta x)dx;$$
(17)

• correlation moment $Q_{L;\pm c}$ that define the excess for the distribution of values $K_{L;\pm C}(\Delta x)$

$$Q_{L;\pm C} = \frac{\sum_{i=1}^{m}\left(K_{L;\pm C}(\Delta x_i)\right)^4}{\sum_{i=1}^{m}\left(K_{L;\pm C}(\Delta x_i)\right)^2}.$$
(18)

The fractal analysis of the distributions $N_{L;\pm C}(x)$ was performed using the calculation of logarithmic dependences $\log J\left[N_{L;\pm C}(x)\right] - \log d^{-1}$ for the power spectra $J\left[N_{L;\pm C}(x)\right]$

$$J = \int_{-\infty}^{+\infty} N_{L;\pm C}\cos 2\pi\nu d\nu ,$$
(19)

where $\nu = d^{-1}$ are the spatial frequencies that are determined by geometrical sizes (d) of PhIL structural elements.

The dependences $\log J\left[N_{L;\pm C}(x)\right] - \log d^{-1}$ are approximated using the least-squares method into the curves $\Phi(\eta)$, straight parts of which serve to determine the slope angles η and calculate fractal F dimensionalities by using the relations [21]

$$F_{L;\pm C} = 3 - tg\eta .$$
(20)

Classification of coordinate distributions $N_{L;\pm C}(x)$ should be performed using the following criteria [22]:

• they are fractal on the condition of a constant slope angle value $\eta = const$ for 2 to 3 decades of changing sizes d;
• they are multi-fractal, if several slope angles $\Phi(\eta)$ are available;
• they are random when any stable slope angles are absent within the whole range of changing sizes d.

In the latter case, the distributions $\log J\left[N_{L;\pm C}(x)\right] - \log d^{-1}$ are characterized with the dispersion

$$D_z = \sqrt{\frac{1}{m}\sum_{i=1}^{m}\left[\log J\left(N_{L;\pm C}(x_i)\right) - \log d^{-1}\right]^2} .$$
(21)

### 5. Characterization of objects under investigation

As objects for these investigations, we used the PhIL samples of the following types:

• PhIL with surface scattering – replicas made of optically isotropic composite resin taken from rough surfaces of the glass K8 ground using free abrasives with statistically averaged sizes of fused alumina grains 5, 10, 28 and 40 μm – group 1;
• PhIL with surface and subsurface scattering – ground surfaces of the glass K8 – group 2;
• PhIL with bulk light scattering – milky glass MC20 of various optical thicknesses with the extinction coefficients $\tau = 1.5, 2.5, 5.0, 10.0$ - group 3.

From the physical viewpoint, this choice of the samples allows to separate and analyze polarization manifestations of various mechanisms providing the scattering of laser radiation that take place both on the surface and in the bulk of PhIL. Besides, one applied aspect – to determine a set of new, polarization-singular criteria allowing to diagnose and differentiate optical properties of theses PhIL within the limits of separate groups.

Fig. 2 illustrates coordinate ($50 pix \times 50 pix$) distributions of the fourth parameter for the Stokes vector $V_4(m \times n)$ inherent to laser images of PhIL in all the groups.

Our qualitative analysis of coordinate distributions $V_4(m \times n)$ for laser images of PhIL (Fig. 2) enabled to reveal:
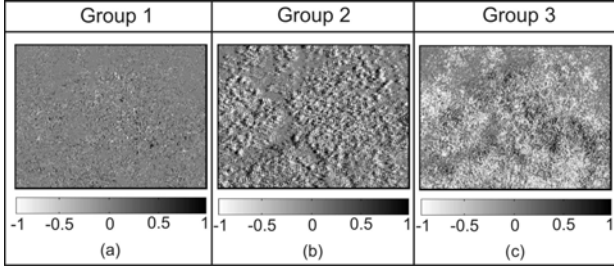
Fig. 2. Coordinate distributions $V_4(m \times n)$ of laser images inherent to PhIL: (a) – replica M28; (b) – ground glass M28; (c) - MC20 ($\tau = 1.5$).

- Practically all the images of the rough surface (Fig. 2a) are linearly polarized field $V_4(m \times n) = 0$ (relations (2) and (3)). Availability of a small amount of the parts $V_4(m \times n) \neq 0$ polarized otherwise can be related with interferential effects of multiple interaction of coherent waves with adjacent micro-roughnesses.
- The image of the K8 glass ground surface (Fig. 2b) is characterized with a developed polarization-inhomogeneous structure formed both by linearly ($V_4(m \times n) = 0$) and elliptically ($V_4(m \times n) \neq 0$) polarized states, including the circularly ($V_4(m \times n) = 1$) polarized ones (relations (5) to (8)).
- The images of the glass MC 20 are characterized with the widest range of changing the azimuth and polarization due to multiple bulk scattering (relations (11) and (12)), - $-1 \leq V_4(m \times n) \leq 1$.

6. Statistical, correlation and fractal analyses for distributions of polarization-singular states in laser images of PhIL

6.1. L states of laser images

Summarized in Fig. 3 is a series of coordinate ($V_4(m \times n) = 0$), quantitative ($N_L(x)$), autocorrelation ($K_L(\Delta m)$) and logarithmic ($\log J_L - \log d^{-1}$) distributions for polarization-singular L states in laser images of PhIL.

Our comparative analysis of the obtained dependences $N_L(x)$ for the amount of polarization-singular L states in laser images of PhIL in all the groups (Figs 3 (d) – (m)) revealed similarity of their statistical, correlation and fractal structures.

For instance, all the $N_L(x)$ distributions are close to the equiprobable ones – the condition $Z_{j=3;4}^L \prec\prec Z_{j=1;2}^L$ is valid for the values of statistical moments (relation (15)). Distinctions between the distributions of L states in laser images of various PhIL are observed as variations of the 1-st and 2-nd statistical moments - $Z_1^L = 0.63; Z_2^L = 0.12; Z_3^L = 0.03; Z_4^L = 0.08$ (group 1);

$Z_1^L = 0.41; Z_2^L = 0.18; Z_3^L = 0.05; Z_4^L = 0.065$ (group 2) and $Z_1^L = 0.18; Z_2^L = 0.29; Z_3^L = 0.02; Z_4^L = 0.08$ (group 3). As seen, for PhIL of the 1-st, 2-nd and 3-rd groups, the mean value Z_1^L is 1.5 and 3.3 times decreased. And vice versa, the dispersion Z_2^L is 1.5 and 2.5 times increased. These changes in $N_L(x)$ distributions are related with the mechanisms of optically-anisotropic (group 2) and interferential phase modulation (group 3) as well as formation (relations (6) and (10)) of elliptically polarized states in laser images of PhIL. Due to these processes, the total amount of polarization L states is decreased with simultaneous conservation of their equiprobable disposition in the image plane of various PhIL.

The investigated statistical structure of L states for polarization of PhIL laser images is confirmed by a monotonous drop of dependences for autocorrelation functions $K_L(\Delta m)$ (relations (16)) of all the distributions $N_L(x)$ (Figs 3(g), (h), (m)). In this case, values of the correlation area S and correlation moment Q trend to their boundary values ($S^L \to 0,33; Q^L \to 0$, relations (17) and (18)) that are characteristic just to equiprobable distributions: $S^L = 0,28; Q^L = 0,09$ (group 1); $S^L = 0,24; Q^L = 0,13$ (group 2) i $S^L = 0,21; Q^L = 0,17$ (group 3).

The performed analysis of logarithmic dependences $\log J_L - \log d^{-1}$ (Figs 3(n), (l), (o)) for the power spectra $J(N_{\pm C})$ (relation (19) of the distribution $N_{\pm C}(x)$ inherent to laser images of the replica taken from the ground glass M28, of the very glass M28 and milky glass MC20 revealed a common regularity – the approximating curves are characterized with stable slope angles that are corresponded with increasing by their value fractal dimensionalities (relation (20)): $F^L = 2.02$ (group 1); $F^L = 2.11$ (group 2) and $F^L = 2.32$ (group 3).
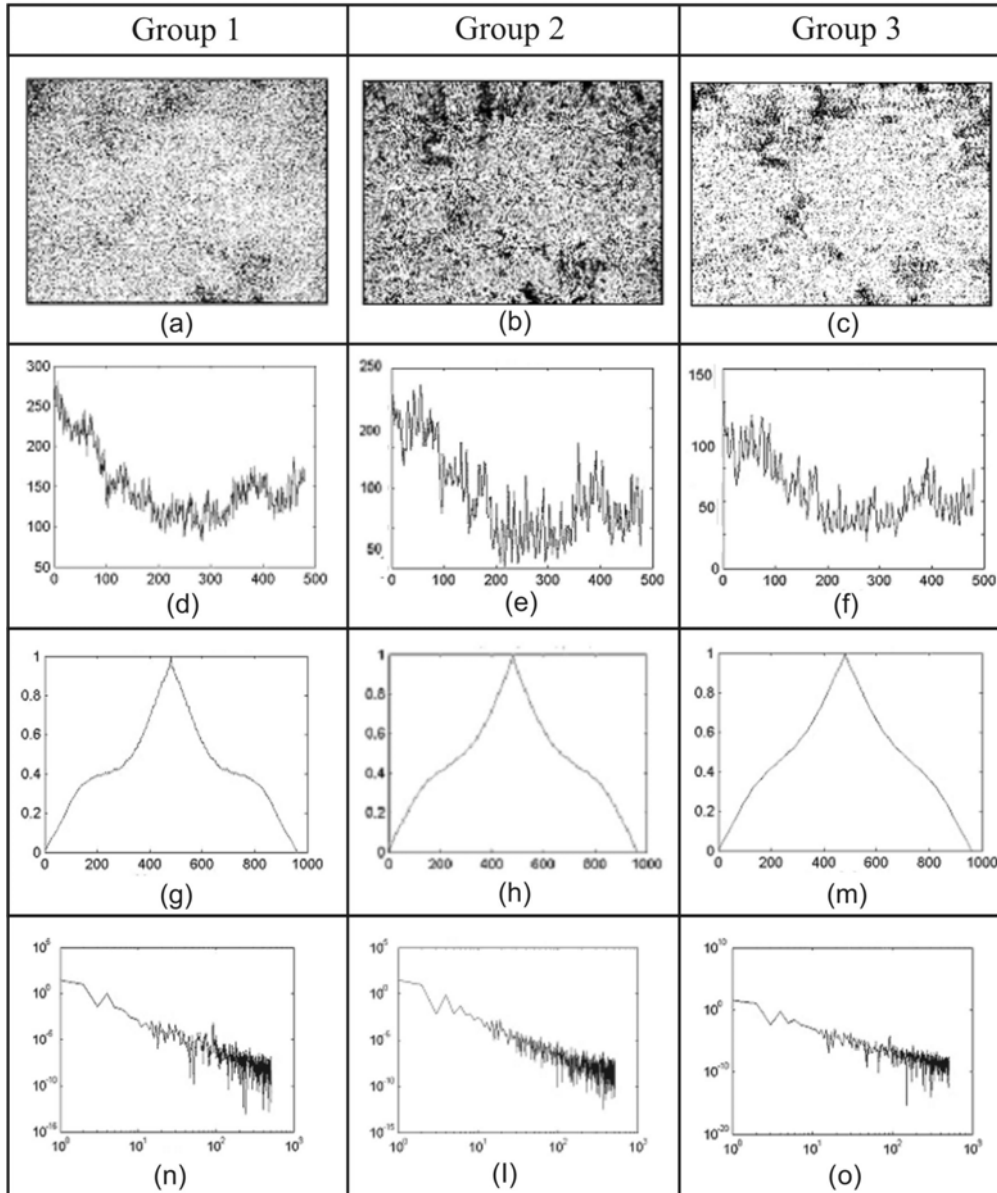
6.2. ±C states of laser images

Summarized in Fig. 4 is the series of coordinate ($V_4(m \times n) = 1$), quantitative ($N_{\pm C}(x)$), autocorrelation ($K_{\pm C}(\Delta m)$) and logarithmic ($\log J_{\pm C} - \log d^{-1}$) distributions for polarization-singular $\pm C -$ states in laser images of PhIL.

In the laser image of the replica taken from the ground glass, $\pm C -$ states of polarization are absent (Fig. 4, left column), which corresponds to model conceptions of mechanisms providing transformation of laser radiation by the set of chaotically oriented micro-areas of the rough surface (relations (1) and (2)).

Optical manifestations of the anisotropic cracked layer are illustrated with the network of $\pm C -$ points in the laser image of ground glass K8 (Fig. 4a). It is seen that

$$V_4(m \times n) = 0$$

Fig. 3. Coordinate $V_4(m \times n) = 0$ ((a), (b), (c)) and quantitative $N_L(x)$ distributions ((d), (e), (f)) of L states in polarization; autocorrelation functions $K_L(\Delta m)$ ((g), (h), (m)) and relations $\log J_L - \log d^{-1}$ ((n), (l), (o)) for power spectra $J(N_L)$ of the distribution $N_L(x)$ for laser images of the replica for the ground glass M28 (left column), ground glass M28 (central column) and milky glass MC20 (right column).

the total amount of circularly polarized points (Fig. 4b) is practically one order less than the amount of linearly polarized states (Fig. 4(c), (d) All the static moments $Z_{j=1;2;3;4}^{\pm C}$ that characterize the distribution $N_{\pm C}(x)$ of the amount of circularly polarized singular states differ from zero: $Z_1^{\pm C} = 0.09; Z_2^{\pm C} = 0.36; Z_3^{\pm C} = 0.44; Z_4^{\pm C} = 0.48$. In this case, the values of statistical moments of higher orders $Z_{j=2;3;4}^{\pm C}$ are commensurable: $Z_2^{\pm C} \approx Z_3^{\pm C} \approx Z_4^{\pm C}$.

This fact is indicative of another, more complex, statistical distribution for the amount of $\pm C$ polarization states as compared with the equiprobable distribution of L polarization states in laser images of the PhIL (group 2).

The autocorrelation function $K^{\pm C}(\Delta m)$ of the dependence $N_{\pm C}(x)$ (Fig. 4e) rapidly drops with increasing the scanning step Δm, which shows the random distribution of states with circular polarization in laser images of the ground PhIL. The correlation area $S^{\pm C}$ and correlation moment $Q^{\pm C}$ of the distribution $N_{\pm C}(x)$ as compared with similar correlation

changes in inverse proportion: $S^{\pm C}(\downarrow) = 0.17$ and $Q^{\pm C}(\uparrow) = 0.97$.

The random character of the $N_{\pm C}(x)$ distribution is also confirmed by the absence of a stable value for the slope angle of the approximating curve to the logarithmic dependence $\log J_{\pm C} - \log d^{-1}$ (Fig. 4g, h). In this case, the dispersion value $D^{\pm C}$ grows up to 2.1
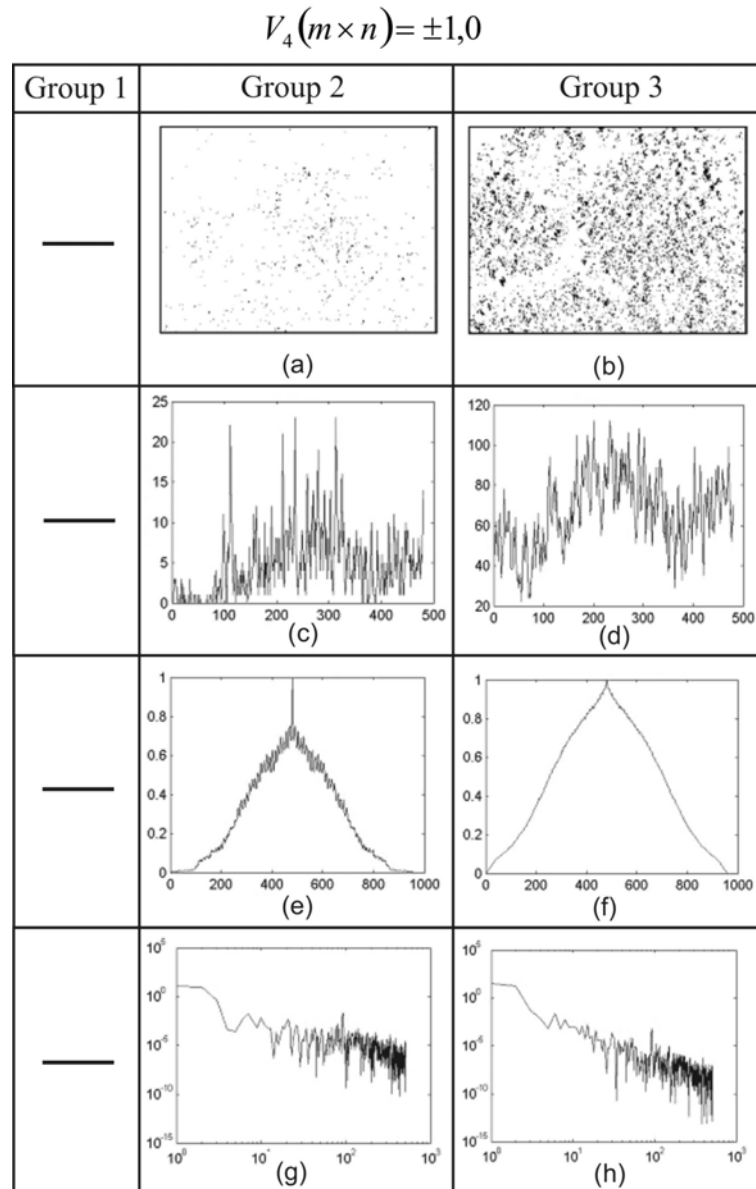
$$V_4(m \times n) = \pm 1,0$$

Fig. 4. Coordinate $V_4(m \times n) = 1$ ((a), (b)), and quantitative $N_L(x)$ distributions ((c), (d)), of $\pm C-$ states in polarization; autocorrelation functions $K_{\pm C}(\Delta m)$ (e), (f), and залежності $\log J_L - \log d^{-1}$ ((g), (h)) for power spectra $J(N_{\pm C})$ of the distribution $N_{\pm C}(x)$ for laser images of the replica for the ground glass M28 (left column), ground glass M28 (central column) and milky glass MC20 (right column).

parameters of $N_L(x)$ distributions (Fig. 3h) experience

times as compared with the data obtained for logarithmic

dependences of power spectra for distributions of the amount of linearly polarized states: $D^{\pm C} = 0.51$.

The phase modulation of multiply scattered laser radiation by the milky glass MC20 is characterized by the network of $\pm C$ − states (Fig. 4b).

The total amount of L- and $\pm C$ − states of polarization for the respective laser image is approximately the same (Figs 3f, 4d). Like to the case of $N_L(x)$ distribution for the amount of linearly polarized states, the $N_{\pm C}(x)$ distribution is close to the equiprobable one: $Z_{j=3;4}^{\pm C} \prec\prec Z_{j=1;2}^{\pm C}$. Differences between statistical moments $Z_{j=1;2;3;4}^{L}$ and $Z_{j=1;2;3;4}^{\pm C}$ are insignificant and lie within 25 to 35 %: $Z_1^{\pm C} = 0.15; Z_2^{\pm C} = 0.34; Z_3^{\pm C} = 0.05; Z_4^{\pm C} = 0.11$.

The values of the correlation area $S^{\pm C}$ and correlation moment $Q^{\pm C}$ are close to their extremum ones: $S^{\pm C} = 0.26; Q^{\pm C} = 0.11$.

Our analysis of the logarithmic dependences (Fig. 4h) for the power spectra $J(N_{\pm C})$ of the $N_{\pm C}(x)$ distribution in laser images of the milky glass MC20 found a stable slope of the approximating curve: $F^{\pm C} = 2.05$. The dispersion value of the distribution $\log J_{\pm C} - \log d^{-1}$ is 1.7 times grown as compared with the analogous statistical moment that characterizes the dependence $\log J_L - \log d^{-1}$ ($D^{\pm C} = 0.26$).

7. Polarization-singular classification and differentiation of optical properties inherent to PhIL

The statistically averaged (within the limits of groups 1 to 3) values and ranges of changing statistical moments $Z_{j=1;2;3;4}^{L;\pm C}$, correlation $Q^{L;\pm C}$, $S^{L;\pm C}$ and fractal $F^{L;\pm C}$, $D^{L;\pm C}$ parameters that characterize the $N_{\pm C}(x)$ dependences for the amount of singular states in laser images of PhIL have been illustrated on Table 1.

The performed analysis of results adduced in Table 1 for statistical ($Z_{j=1;2;3;4}^{L;\pm C}$), correlation ($S^{L;\pm C}; Q^{L;\pm C}$) and fractal ($F^{L;\pm C}; D^{L;\pm C}$) parameters has shown:

1. *For PhIL of the group 1*:

- differentiation of optical properties inherent to rough surfaces with different micro-relief parameters is possible when using determination of values for the 2-nd and 4-th statistical moments of the distribution specific to the amount of L polarization states: with increasing the micro-relief, the value Z_2^{L} grows by 1.85 times, while the value Z_4^{L} is 2.3 times lowered;

- the dispersion value D^{L} for the distribution of extremes in logarithmic dependences $\log J_L - \log d^{-1}$ describing laser images of large-scale (M40) rough surfaces is 2.2 times increased;

- the values of correlation parameters ($S^{L;\pm C}; Q^{L;\pm C}$) that characterize the dependences $N_L(x)$ for laser images of surfaces with various sizes of micro-roughness (from 1 to 40 μm) cannot serve as reliable criteria for their differentiation.

2. *For PhIL of the group 2*:

- the variations of values inherent to all the statistical moments $Z_{j=1;2;3;4}^{\pm C}$ that characterize the distribution of the amount of $\pm C$ − states in the respective laser images were found to be sensitive to changes in the thickness of top and subsurface layers on surfaces ground with abrasive powders M5, M10, M28 and M40: when sizes of fused alumina grow, $Z_1^{\pm C}$ is 1.6 times decreased; $Z_2^{\pm C}$ is 2.1 times increased; $Z_3^{\pm C}$ increases by 1.8 times and $Z_4^{\pm C}$ is 3.2 times increased;

- there observed are significant differences between the values of correlation areas $S^{\pm C}$ (1.7 times growth) and correlation moments $Q^{\pm C}$ (2.9 times drop);

Table 1. Statistical, correlation and fractal parameters for the distribution of the amount of polarization-singular states in laser images of PhIL

Parameters ($L-; \pm C-$)	Rough surfaces		Ground surfaces		Bulk PhIL	
	$L-$	$\pm C-$	$L-$	$\pm C-$	$L-$	$\pm C-$
Z_1	0.72 ± 0.077	−	0.45 ± 0.05	0.12 ± 0.034	0.24 ± 0.038	0.23 ± 0.045
Z_2	0.11 ± 0.037	−	0.21 ± 0.041	0.38 ± 0.093	0.31 ± 0.053	0.25 ± 0.032
Z_3	0.04 ± 0.005	−	0.06 ± 0.008	0.48 ± 0.11	0.03 ± 0.005	0.07 ± 0.009
Z_4	0.15 ± 0.049	−	0.09 ± 0.01	0.52 ± 0.28	0.07 ± 0.05	0.09 ± 0.06
S	0.29 ± 0.02	−	0.25 ± 0.021	0.19 ± 0.052	0.23 ± 0.031	0.25 ± 0.029
Q	0.07 ± 0.008	−	0.09 ± 0.0089	1.12 ± 0.54	0.15 ± 0.042	0.13 ± 0.018
F	2.05 ± 0.12	−	2.15 ± 0.014	−	2.36 ± 0.09	2.09 ± 0.11
D	0.23 ± 0.083	−	0.25 ± 0.014	0.45 ± 0.023	0.21 ± 0.018	0.24 ± 0.018

- $N^{\pm C}$ distributions for the amount of $\pm C$ – states in laser images of all the ground surfaces are statistical – the approximating curves for the dependences $\log J_{\pm C} - \log d^{-1}$ have no stable slope;

- the dispersion value $D^{\pm C}$ for the logarithmic dependences of power spectra for the $N^{\pm C}$ distributions is changed insignificantly (by 1.1 times) and cannot serve as a reliable criterion for differentiation of optical properties of ground surfaces.

   3. *For PhIL of the group 3*:

- there exists a possibility to use statistical moments of the 4-th order that characterize the $N^L(x)$ and $N^{\pm C}(x)$ distributions for differentiation of optically-thick layers with a bulk scattering: with increasing the optical thickness, the differences between Z_4^L and $Z_4^{\pm C}$ reach 6 and 5 times, respectively;

- weak differences take place between the values of correlation parameters $S^{L;\pm C}; Q^{L;\pm C}$: 1.25 and 1.4 times, respectively;

- $N^L(x)$ and $N^{\pm C}(x)$ distributions are fractal.

   4.   *For PhIL of all the groups*:

The possibility to differentiate "group" optical properties of PhIL with surface, subsurface and bulk light scattering is illustrated in Table 2.

Table 2.

PhIL Parameters	Groups 1 – 3	
	N_L	$N_{\pm C}$
Z_1	$\oplus$	$\oplus$
Z_2	$\oplus$	$\oplus$
Z_3	$\otimes$	$\oplus$
Z_4	$\otimes$	$\oplus$
S	$\otimes$	$\oplus$
Q	$\otimes$	$\oplus$
F	$\otimes$	$\oplus$
D	$\otimes$	$\oplus$

Note: $\otimes$ - here differentiation is impossible; $\oplus$ - possible.

8. Conclusions

1.   Analyzed in this work are the main physical mechanisms providing formation of polarization singularities in laser images of PhIL with surface, subsurface and bulk light scattering.

2.   Offered are statistical, correlation and fractal parameters for polarization-singular estimating the optical properties inherent to PhIL of all types.

3.   Determined are the ranges for changing the set of criteria that characterize distributions of the amount of polarization-singular states in laser images, which enabled us to realize both "intergroup" classification and "intragroup" differentiation of optical properties related to PhIL of various types.

References

1. Wang X. Monte Carlo model and single-scattering approximation of polarized light propagation in turbid media containing glucose / X. Wang, G. Yao, L. - H. Wang // Appl. Opt. – 2002. – Vol. 41. – P. 792–801.

2. Wang X. Propagation of polarized light in birefringent turbid media: a Monte Carlo study / X. Wang, L. - H. Wang // J. Biomed. Opt. – 2002. – Vol. 7. – P. 279-290.

3. Handbook of Optical Coherence Tomography; edited by B.E. Bouma and G.J. Tearney // Polarization-sensitive optical coherence tomography / J. F. de Boer, T. E. Milner, M. G. Ducros, S. M. Srinivas and J. S. Nelson. – Marcel Dekker Inc.: New York, 2002. – P. 237-274.

4. Everett M. J. Birefringence characterization of biological tissue by use of optical coherence tomography / M. J. Everett, K. Shoenenberger, B. W. Colston, L. B. Da Silva // Opt. Lett. – 1998. – Vol. 23. – P. 228-230.

5. Gang Yao. Two-dimensional depth-resolved Mueller matrix characterization of biological tissue by optical coherence tomography / Gang Yao, Lihong V. Wang // Opt. Lett. – 1999. – Vol. 24. – P. 537-539.

6. Shuliang Jiao. Depth-resolved two-dimensional Stokes vectors of backscattered light and Mueller matrices of biological tissue measured with optical coherence tomography / Shuliang Jiao, Gang Yao, Lihong V. Wang // Appl. Opt. – 2000. – Vol. 39. – P. 6318-6324.

7. Shuliang Jiao. Two-dimensional depth-resolved Mueller matrix of biological tissue measured with double-beam polarization-sensitive optical coherence tomography / Shuliang Jiao, Lihong V. Wang // Opt. Lett. – 2002. – Vol. 27. – P. 101-103.

8. Wang X. Polarized light propagation through the scattering media: time-resolved Monte Carlo and experiments / X. Wang, L. - H. Wang, C. - W. Sun, C. C. Yang // J. Biomed. Opt. – 2003. – Vol. 8. – P. 608-617.

9. Demos S. G. Optical polarization imaging / S. G. Demos, R. R. Alfano // Appl. Opt. – 1997. –Vol. 36. – P. 150-155.

10. Ducros M. G. Polarization sensitive optical coherence tomography of the rabbit eye / M. G. Ducros, J. F. de Boer, H. E. Huang, L. C. Chao, Z. P.Chen, J. S. Nelson, T. E. Milner, H. G. Rylander // IEEE J. Select. Top. Quant. Electron. – 1999. – Vol. 5. – P. 1159-1167.

11. de Boer Johannes F. Two-dimensional birefringence imaging in biological tissue using polarization-sensitive optical coherence tomography / Johannes F. de Boer, Thomas E. Milner, Martin J. van Gemert, John S. Nelson, John S // Proc. SPIE. – 1998. – Vol. 3196. – P. 32-37.

12. J. F. de Boer. Determination of the depth-resolved Stokes parameters of light backscattered from turbid media by use of polarization-sensitive optical coherence tomography / J. F. de Boer, T. E. Milner, J. S. Nelson // Opt. Lett. – 1999. – Vol. 24. – P. 300-302.

13. Mandelbrot B. B. The Fractal Geometry of Nature / Mandelbrot B. B. – San Francisco: W.H.Freeman, 1982. – 460 p.

14. Freund Isaac. Elliptic critical points in paraxialoptical fields / Isaac Freund, Marat S. Soskin, Alex I. Mokhun // Optics Communications. – 2002. – Vol. 207. – P. 223-253.

15. Soskin M. S. Optical polarization singularities and elliptic stationary points / M. S. Soskin, V. Denisenko, I. Freund // Opt. Lett. – 2003. – Vol. 28. – P. 1475-1477.

16. Dennis M. R. Polarization singularities in paraxial vector fields: morphology and statistics / M.R. Dennis // Opt. Commun. – 2002. – Vol. 213. – P. 201-221.

17. Soskin M. S. Singular elliptic light fields: genesis of topology and morphology / M. S. Soskin, V. G. Denisenko, R. I. Egorov // Proc. SPIE. – 2006. – Vol. 6254. – P. 625404.

18. Nye J.F. Lines of circular polarization in electromagnetic wave fields / J. F. Nye // Proc. R. Soc. Lond. – 1983. – A. 389. – P. 279-290.

19. Flossmann F. Polarization singularities from unfolding an optical vortex through a birefringent crystal / F. Flossmann, U. T. Schwarz, M. Maier, M. R. Dennis // Phys. Rev. Lett. – 2005. – Vol. 95. – P. 253901.

20. Flossmann F. Stokes parameters in the unfolding of an optical vortex through a birefringent crystal / F. Flossmann, U. T. Schwarz, M. Maier, M. R. Dennis // Opt. Express. – 2006. – Vol. 14. – P. 11402-11411.

21. Bliokh K. Y. Singular polarimetry: Evolution of polarization singularities in electromagnetic waves propagating in a weakly anisotropic medium / K.Y. Bliokh, A. Niv, V. Kleiner, E. Hasman // Opt. Express. – 2008. – Vol. 16. – P. 695-709.

22. Freund I. Stokes singularity relations / I. Freund, A. I. Mokhun, M. S. Soskin, O. V. Angelsky, I. I. Mokhun // Optics Letters. – 2002. – Vol. 27, № 7. – P. 545-547.

23. Alexander G. Ushenko and Vasilii P. Pishak, "Laser Polarimetry of Biological Tissue: Principles and Applications", in *Handbook of Coherent-Domain Optical Methods: Biomedical Diagnostics, Environmental and Material Science*, Vol. 1, pp. 93-138, edited by Valery V. Tuchin, Kluwer Academic Publishers, 2004.

24. A.G. Ushenko, "Stokes-correlometry of biotissues," Laser Physics, vol. 10(5), pp.1286-1292, 2000.

25. A.G. Ushenko, "The Vector Structure of Laser Biospeckle Fields and Polarization Diagnostics of Collagen Skin Structures," Laser Physics, vol. 10(5), pp. 1143-1149, 2000.

26. A.G. Ushenko, I. Z.Misevich, V. Istratiy, I. Bachyns'ka, A. P. Peresunko, Omar Kamal Numan, and T. G. Moiysuk, "Evolution of Statistic Moments of 2D-Distributions of Biological Liquid Crystal Net Mueller Matrix Elements in the Process of Their Birefringent Structure Changes," Advances in Optical Technologies, vol. 2010, Article ID 423145, 2010.

27. O. V. Dubolazov, A. G. Ushenko, V. T. Bachynsky, A. P. Peresunko, and O. Ya. Vanchulyak, "On the Feasibilities of Using the Wavelet Analysis of Mueller Matrix Images of Biological Crystals," Advances in Optical Technologies, vol. 2010, Article ID 162832, 2010.

28. O.V. Angelsky, A.G. Ushenko, Ye.G. Ushenko, "2-D Stokes Polarimetry of Biospeckle Tissues Images in Pre-Clinic Diagnostics of Their Pre-Cancer States," Journal of Holography and Speckle, vol. 2(1), pp.26-33, 2005.

29. A.G. Ushenko, "Laser diagnostics of biofractals," Quantum Electronics, vol. 29(12), pp. 1078–1084, 1999.

30. O.V. Angel'skii, A.G. Ushenko, A.D. Arkhelyuk, S.B. Ermolenko, D.N. Burkovets, "Structure of matrices for the transformation of laser radiation by biofractals," Quantum Electronics, vol. 29(12), pp. 1074-1077, 1999.

31. O.V. Angel'skii, A.G. Ushenko A.D. Arheluk, S.B. Ermolenko, D. N. Burkovets, "Scattering of Laser Radiation by Multifractal Biological Structures," Optics and Spectroscopy, vol. 88(3), pp. 444-448, 2000.

32. A.G. Ushenko, "Polarization Structure of Biospeckles and the Depolarization of Laser Radiation," Optics and Spectroscopy, vol. 89(4), pp. 597-601, 2000.

33. A.G. Ushenko, "Laser polarimetry of polarization-phase statistical moments of the object field of optically anisotropic scattering layers," Optics and Spectroscopy, vol. 91(2), pp. 313-316 2001.

34. A.G. Ushenko, "Polarization contrast enhancement of images of biological tissues under the conditions of multiple scattering," Optics and Spectroscopy, vol. 91(6), pp. 937-940, 2001.

35. A.G. Ushenko, "Laser probing of biological tissues and the polarization selection of their images," Optics and Spectroscopy, vol. 91(6), pp.932-936, 2001.

36. A.G. Ushenko, "Correlation processing and wavelet analysis of polarization images of biological tissues," Optics and Spectroscopy, vol. 91(5), pp.773-778, 2002.

37. A.G. Ushenko, "Polarization correlometry of angular structure in the microrelief pattern or rough surfaces," Optics and spectroscopy, vol. 92(2), pp.227-229, 2002.

38. Oleg V. Angelsky, Alexander G. Ushenko, and Yevheniya G. Ushenko, "Complex degree of mutual polarization of biological tissue coherent images for the diagnostics of their physiological state," J. Biomed. Opt., vol. 10(6), 060502, 2005.

39. Oleg V. Angelsky, Alexander G. Ushenko, Yevheniya G. Ushenko, Yuriy Y. Tomka, "Polarization singularities of biological tissues images," J. Biomed. Opt., vol. 11(5), 054030, 2006.

40. Alexander G. Ushenko, "Polarization structure of laser scattering fields," Optical Engineering, vol. 34(4), pp. 1088-1093, 1995.

41. A.G. Ushenko, M.T. Strinadko, S.B. Yermolenko, M.A Neduzhko, "High resolution polarization interferometry in surface and layer diagnostics," International journal of optoelectronics, vol. 4(6), pp. 563–574, 1989.

42. O. V. Angelsky, A. G. Ushenko, and Ye. G. Ushenko, "Investigation of the correlation structure of biological tissue polarization images during the diagnostics of their oncological changes," Phys. Med. Biol., vol. 50, pp. 4811-4822, 2005.

43. O.G. Ushenko, S.G. Guminetsky, A.V. Motrich, "Optical properties of urine, blood plasma and pulmonary condensate of the patients with pulmovnary form of tuberculosis," Fotoelektronika, vol.16, pp. 133-139, 2007.